

Nonclassical light generation by a photonic-crystal one-atom laser

Lucia Florescu*

Jet Propulsion Laboratory, California Institute of Technology, Mail Stop 126-347, 4800 Oak Grove Drive, Pasadena, California 91109-8099, USA

(Received 4 April 2008; published 15 August 2008)

We investigate the effects of sub-Poissonian photon statistics and photon antibunching in the light generation by a photonic-crystal one-atom laser. The physical system consists of a two-level light emitter strongly coupled to a high-quality microcavity engineered within a photonic crystal and coherently driven by a strong external laser field. This study reveals that the electromagnetic environment provided by the photonic crystal facilitates light generation characterized by pronounced sub-Poissonian photon statistics and photon antibunching, and strongly enhanced relative to that from a one-atom laser in a conventional optical cavity. The characteristics of the cavity photon statistics are fundamentally distinct from those of a corresponding microcavity in ordinary vacuum. For large discontinuities in the photon density of states between Mollow spectral components of atomic resonance fluorescence, in the good cavity regime, the photon statistics is sub-Poissonian, in contrast to the case of a conventional cavity where sub-Poissonian photon statistics is present only for a bad cavity. These results suggest the possibility of using a photonic-crystal one-atom laser as an efficient source of nonclassical light.

DOI: [10.1103/PhysRevA.78.023827](https://doi.org/10.1103/PhysRevA.78.023827)

PACS number(s): 42.55.Tv, 42.50.Ar

I. INTRODUCTION

The system of an atom or a quantum dot interacting with the quantized field of a high- Q microcavity represents an important tool for the investigation of quantum electrodynamic effects. The possibility of realizing high- Q cavities both in optical and microwave regimes has enabled the observation of a number of remarkable effects, including vacuum Rabi splitting [1], photon antibunching [2], and conditional phase shifts for quantum logic gates [3]. Recently, a one-atom laser consisting of a single atom trapped inside a high-quality factor microcavity and externally pumped has been realized [4]. It was shown that the characteristics of the pumped atom-cavity system are qualitatively different from those of the familiar many-atom lasers. In particular, this one-atom laser produces nonclassical light and can act as an efficient source for deterministic generation of single-photon pulses [5].

On the other hand, new studies of quantum electrodynamic phenomena are facilitated by optical microcavities engineered in photonic crystals [6,7]. The advantage of using photonic-crystal microcavities for cavity QED studies stems from their ability to simultaneously realize extremely small microcavity mode volumes and very high cavity Q factors, which are the key ingredients for realizing strong atom-cavity coupling. For instance, in a two-dimensional (2D) photonic crystal, a microlaser with a cavity volume of 0.03 cubic microns has been demonstrated [8]. Within a three-dimensional (3D) photonic band gap (PBG) with complete light localization [9,7], there is no fundamental upper bound to the microcavity Q factor. Moreover, new effects in the dynamics of the atom-cavity system are also facilitated by the surrounding electromagnetic environment provided by

the photonic crystal. One of the key features that distinguishes the photonic radiation reservoir associated with a photonic crystal from its free space counterpart is that the photonic density of states (DOS) within or near a photonic band gap or low-DOS region can nearly vanish or exhibit discontinuous changes as a function of frequency with appropriate engineering. This property enables new optical phenomena, such as photon-atom bound states [10], fractionalized single-atom inversion [11], optical bistability and switching in multiatom systems [12], or coherent control of spontaneous emission through quantum interference [13].

Recently, a proposal for a photonic-crystal one-atom laser consisting of a coherently pumped single atom or quantum dot strongly coupled to an optical cavity engineered in a PBG microchip was put forward [14], and new one-atom laser features have been predicted. In particular, strong enhancement of the cavity field relative to that of a cavity in ordinary vacuum, better coherence [14], as well as fundamentally new spectral features of the cavity field [15] have been theoretically demonstrated for the case of a cavity tuned on resonance with the central component of Mollow resonance fluorescence spectrum. These effects result from the ability to engineer high- Q cavities and high electromagnetic field distributions as well as large discontinuities in the density of states of the surrounding electromagnetic reservoir.

On the experimental front, remarkable progress in coupling single quantum dots to a photonic-crystal microcavity has been made recently. Significant modification of the spontaneous emission and photon antibunching have been demonstrated for single emitters embedded in a photonic-crystal microcavity [16]. Also, deterministic coupling a single quantum dot to a photonic-crystal cavity has been realized [17], and a thresholdless laser operating on a single quantum dot is expected to be achieved [18]. Moreover, the recent advances [19] in the fabrication of 2D-3D-2D photonic-crystal architectures [20] may enable the realization of a one-atom laser in photonic structures characterized by large variation with frequency of the photonic density of states.

*Present address: Department of Bioengineering, University of Pennsylvania, Philadelphia, PA 19104.

This work addresses the problem of nonclassical light generation by a photonic-crystal one-atom laser. This is of relevance for both understanding the quantum features of light-matter interaction in structured photonic reservoirs as well as for applications in quantum-information technology. Although previous theoretical studies [14,15] have demonstrated the advantage of using photonic-crystal cavities for enhanced, coherent, spectrally narrower one-atom laser emission, the laser system consisting of a coherently pumped two-level atomic system strongly coupled to a photonic cavity resonant with the central component of Mollow atomic fluorescence spectrum considered in these studies does not facilitate nonclassical light generation. Nonclassical states of light may be produced in such photonic-crystal microcavities if a four-level emitter and a more complex pumping mechanism are used, similarly to the conventional one-atom laser [4,5]. Here, we consider a different approach and propose a one-atom laser system in which a coherently pumped two-level system is strongly coupled to a cavity field tuned on resonance with one of the side components of Mollow atomic resonance fluorescence spectrum. This approach has the advantage of avoiding the necessity of manipulating multiple pump laser beams or of preparing the atomic system. Also, using two-level emitters may result in faster light generation. Given the different origin and characteristics of the the Mollow spectral components, it is expected that this laser system have different dynamics from that proposed in Ref. [14]. We investigate the nonclassical effects of sub-Poissonian photon statistics and photon antibunching in the light emission by this laser device and show that the emitted light has distinct characteristics from those corresponding to a conventional cavity. In a photonic crystal, in the good cavity limit and for strong atom-cavity coupling, the strong enhancement of the cavity field relative to that of a conventional cavity is accompanied by pronounced sub-Poissonian statistics. This is in contrast to the case of a conventional cavity, when the cavity field exhibits super-Poissonian photon statistics. Also, photon antibunching is unveiled for both conventional and photonic-crystal cavities, the time scale for which the antibunching is observed being larger in photonic-crystal structures. These results suggest the advantage of using photon-crystal cavities for nonclassical light generation.

II. MODEL

The model for a one-atom laser in photonic crystals has been introduced in Ref. [14]. It consists of a single two-level atom driven by a coherent external laser field and coupled to a high- Q microcavity engineered within a photonic crystal. Such a system can be realized, for instance, by embedding a quantum dot in a dielectric microcavity (point defect) placed within a two-mode waveguide channel (linear defect) in a 2D PBG microchip [14]. One mode of the waveguide channel is engineered to produce a large discontinuity in the local photon density of states (LDOS) at a certain frequency, and another mode is used to propagate the pump beam. By suitable engineering of the system topology, it is possible to tailor the electromagnetic field distribution to realize a strong coupling of the light emitter to both the pumping waveguide mode and

the high- Q cavity mode [14]. Moreover, the cavity resonant frequency can be engineered to be within a photonic band-gap or low-LDOS region and near the LDOS discontinuity, such that the atomic system that is strongly coupled to the cavity field also experiences this discontinuity that strongly influences the atom dynamics and results in new emission effects. By further sandwiching the 2D microchip between two 3D PBG cladding layers above and below, a factor of 100 jump in the photonic density of states can be achieved [21].

The atom has excited state $|2\rangle$, ground state $|1\rangle$, and resonant transition frequency ω_a . The coupling constant between the atomic transition and the microcavity mode is given by $g = (\omega_a d_{21} / \hbar) (\hbar / 2 \epsilon_0 \omega_c V)^{1/2} \mathbf{e} \cdot \mathbf{u}_d$, where d_{12} and \mathbf{u}_d are the absolute value and the unit vector of the atomic dipole moment, V is the volume of the cavity mode, \mathbf{e} is the polarization mode of the cavity radiation field, ϵ_0 is the Coulomb constant, and \hbar is the reduced Planck constant. In the optical regime, dipole moments of $d_{21} \approx 10^{-29}$ C m and a microcavity mode volume of $V \approx (1 \mu\text{m})^3$ as experimentally realized [8,22] yield a coupling constant of the order $g \approx 10^{-5} \omega_a$. The atom is driven near resonance by a coherent external field at a frequency ω_L and Rabi frequency $\varepsilon = d_{12} E / \hbar$ (where E is the field amplitude). For simplicity, we treat the driving field classically and work in the interaction picture. The excited atomic system decays by spontaneous emission into the modes of the radiation reservoir associated with the engineered photonic crystal. The dephasing of the atomic system, which may arise from scattering of phonons of the host crystal on the atom embedded in the solid part of the dielectric material, takes place at a rate γ_p , and the cavity field is damped at the rate κ , caused by the extraneous coupling of the cavity mode to the engineered waveguide modes or possible leakage of light from the microcavity in the vertical direction. In this study, the rates γ_p and κ are introduced phenomenologically.

In order to investigate the emission characteristics, it is useful to use the dressed states, $\{|\tilde{i}\rangle\}_{i=1,2}$ [12,23], which are the states of the atomic system dressed by the driving field. These states are related to the atomic bare states $\{|i\rangle\}_{i=1,2}$ through

$$|\tilde{1}\rangle = c|1\rangle - s|2\rangle, \quad (2.1)$$

$$|\tilde{2}\rangle = s|1\rangle + c|2\rangle. \quad (2.2)$$

Here, $c \equiv \cos(\phi)$, $s \equiv \sin(\phi)$, with ϕ the rotation angle that belongs in the interval $[0, \pi]$ and is defined by

$$\cos^2 \phi = \frac{1}{2} \left(1 + \frac{\Delta_a}{\Omega} \right). \quad (2.3)$$

Here

$$\Omega = (4\epsilon^2 + \Delta_a^2)^{1/2} \quad (2.4)$$

is the generalized Rabi frequency, and $\Delta_a = \omega_a - \omega_L$ is the detuning of the atomic resonance frequency from the pump laser frequency. The corresponding dressed-state atomic operators $R_{ij} = |\tilde{i}\rangle\langle\tilde{j}|$ ($i, j = 1, 2$) are related to the bare state

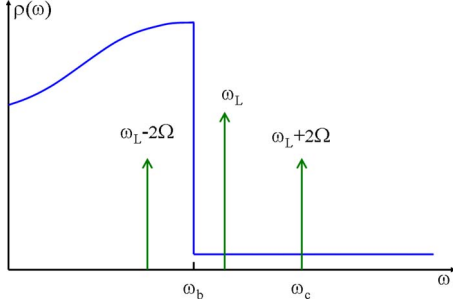


FIG. 1. (Color online) Schematic representation of the photonic DOS $\rho(\omega)$ and the relative position of the relevant frequencies considered in our study. ω_L and ω_c are the frequency of the coherent pump field and microcavity field frequency, respectively. The vertical arrows represent the emission lines of the Mollow spectrum of atomic resonance fluorescence, with the central band occurring at the frequency ω_L , and the side bands components at $\omega \pm 2\Omega$ (Ω is the generalized Rabi frequency). The continuous line represents the photonic DOS showing rapid variation with the frequency near a photonic band-edge frequency ω_b . In ordinary vacuum, the photonic DOS is featureless and approximately constant over the frequency range of interest.

atomic operators $\sigma_{ij} = |i\rangle\langle j|$ according to the transformation,

$$\sigma_{12} = \frac{1}{2} \sin(2\phi)R_3 - \sin^2\phi R_{21} + \cos^2\phi R_{12}, \quad (2.5a)$$

$$\sigma_{22} - \sigma_{11} = \cos(2\phi)R_3 - \sin(2\phi)(R_{12} + R_{21}), \quad (2.5b)$$

$$R_3 = R_{22} - R_{11}. \quad (2.5c)$$

For a strong monochromatic driving field oscillating on or near resonance to an atomic transition, the dressed atom states are grouped in manifolds, each manifold consisting of two states, $|\tilde{i}, n\rangle$, $i=1, 2$ (where n is the number of photons in the driving field) [24]. The eigenenergies of each manifold increase with n , the splitting between the states of a given manifold is $\hbar\Omega$, and the splitting between similar states in successive manifolds is $\hbar\omega_L$. The transitions between the states $|i, n+1\rangle$ of one manifold and the states $|j, n\rangle$ of the manifold below give rise to the triplet resonance fluorescence Mollow spectrum, with spectral lines at ω_L and $\omega_L \pm 2\Omega$ [25].

A general master equation for the density operator of the system of atom plus cavity, ρ has been derived in Ref. [14] in the secular [26] and Born-Markov [27] approximations. These standard approximations in quantum optics have been applied with considerable success to a variety of atom-field interaction problems in photonic crystals [11,28]. The Born approximation assumes a weak coupling between the atomic system and the radiation reservoir of the photonic crystal and also that changes in the photonic reservoir as a result of atom-reservoir interaction are negligible. The Markov approximation assumes a fast time scale for the decay of the reservoir correlations. In our case, this results from the assumption that the photonic density of modes is constant over the spectral regions surrounding the dressed-state resonant frequencies. The secular approximation is based on the as-

sumption that the driving field is strong enough, such that the generalized Rabi frequency Ω is much larger than the relevant decay rates. The validity of these approximations for the case of a photonic crystal was discussed in detail in Refs. [11,28,14]. Also, it is considered that the phonon, cavity, and photonic reservoirs are statistically independent, and that the phonon DOS is broad and displays no sharp features. Thus, the part of the master equation describing the dephasing of the atomic system has the usual form [27] $(\partial\rho/\partial t)_{\text{dephase}} = \gamma_p(\sigma_3\rho\sigma_3 - \rho)$. The master equation for the atom-cavity field system in the dressed-state basis is [14]

$$\begin{aligned} \frac{\partial\rho}{\partial t} = & g\{sc[a^\dagger R_3 e^{i\Delta_c t} - R_3 a e^{-i\Delta_c t}, \rho] \\ & + c^2[a^\dagger R_{12} e^{i(\Delta_c - 2\Omega)t} - R_{21} a e^{-i(\Delta_c - 2\Omega)t}, \rho] \\ & - s^2[a^\dagger R_{21} e^{i(\Delta_c + 2\Omega)t} - R_{12} a e^{-i(\Delta_c + 2\Omega)t}, \rho]\} \\ & + \left\{ \frac{A_0}{2}[R_3\rho R_3 - \rho] + \frac{A_-}{2}[R_{21}\rho R_{12} - R_{11}\rho] \right. \\ & \left. + \frac{A_+}{2}[R_{12}\rho R_{21} - R_{22}\rho] + \text{H.c.} \right\} \\ & + \frac{\kappa}{2}[2a\rho a^\dagger - a^\dagger a\rho - \rho a^\dagger a]. \end{aligned} \quad (2.6)$$

The first group of terms in the master equation (2.6) corresponds to the interaction between the dressed atomic system and the cavity mode, and the second group of terms describes the spontaneous emission of the dressed atom into the modes of the photonic-crystal radiation reservoir. In particular, the term containing A_- corresponds to the atomic spontaneous decay from the lower dressed state $|\tilde{1}\rangle$ of one manifold to the upper dressed state $|\tilde{2}\rangle$ of the manifold below, while the term containing A_+ describes the spontaneous decay from the excited dressed state $|\tilde{2}\rangle$ of one manifold to the lower dressed state $|\tilde{1}\rangle$ of the manifold below [24,29]. In Eq. (2.6), $A_0 = \gamma_0 s^2 c^2 + \gamma_p(c^2 - s^2)$, $A_- = \gamma_- s^4 + 4\gamma_p s^2 c^2$, and $A_+ = \gamma_+ c^4 + 4\gamma_p s^2 c^2$, and spontaneous emission decay rates $\gamma_0 = 2\pi \sum_\lambda g_\lambda^2 \delta(\omega_\lambda - \omega_L)$, $\gamma_- = 2\pi \sum_\lambda g_\lambda^2 \delta(\omega_\lambda - \omega_L + 2\Omega)$, and $\gamma_+ = 2\pi \sum_\lambda g_\lambda^2 \delta(\omega_\lambda - \omega_L - 2\Omega)$ are proportional to the density of modes at the dressed-state transition frequencies ω_L , $\omega_L - 2\Omega$, and $\omega_L + 2\Omega$, respectively. Note that the effect of the atomic dephasing due to phonons is to increase the decay rates A_\pm relative to the case when no dipolar dephasing is present, while decreasing A_0 for negative atom-field detuning, $\Delta_a < 0$, and increasing it for $\Delta_a > 0$. In Eq. (2.6), g_λ is the coupling constant between the atom and the mode λ of frequency ω_λ of the radiation field of the photonic reservoir, and $\Delta_c = \omega_c - \omega_L$, is the detuning of the cavity-mode frequency ω_c from the pump laser frequency. The model photonic density of states as a function of frequency presenting a discontinuity near a band-edge frequency, and the relevant frequencies for this study and their relative position are presented in Fig. 1. The strong driving field intensity determines a relatively large Mollow splitting, such that the spectral components of the Mollow triplet are pushed away from the DOS discontinuity and experience different densities of

states (and, implicitly, different spontaneous rates, γ_0, γ_{\pm}). This is in contrast to the case of ordinary vacuum, where the photonic DOS as a function of frequency is broad and slowly varying, and can be considered almost constant over the frequency range spanned by the Mollow transition frequencies. For $\gamma_0 = \gamma_+ = \gamma_- = \gamma$ (where γ is the atom spontaneous emission rate in free space), Eq. (2.6) describes a one-atom laser in a conventional cavity [23]. The last group of terms describes the damping of the cavity mode via cavity decay. Within the secular approximation that we use here, the generalized Rabi frequency Ω is assumed much larger than the decay rates $\gamma_0, \gamma_+, \gamma_-$, and κ . We note that although the driving fields are assumed strong, the strong subwavelength focusing of the optical beam by the photonic-crystal waveguide enables relatively low power levels [30].

We consider here the case of the cavity field tuned to resonance with the Mollow high-frequency sideband, corresponding to $\Delta_c = 2\Omega$. We note that the tuning of the cavity field on resonance with the Mollow low-frequency sideband, $\Delta_c = 2\Omega$, will produce the same results for $\Delta_a \rightarrow -\Delta_a$ and $\gamma_- \rightarrow \gamma_+$. Assuming a strong pump field, one can invoke the secular approximation to ignore the rapidly oscillating terms at frequencies 2Ω and 4Ω in the master equation (2.6). The master equation (2.6) reduces in this case to

$$\begin{aligned} \frac{\partial \rho}{\partial t} = & g_1 [a^\dagger R_{12} - R_{21} a, \rho] + \left\{ \frac{A_0}{2} [R_3 \rho R_3 - \rho] \right. \\ & + \frac{A_-}{2} [R_{21} \rho R_{12} - R_{11} \rho] + \frac{A_+}{2} [R_{12} \rho R_{21} - R_{22} \rho] + \text{H.c.} \left. \right\} \\ & + \frac{\kappa}{2} [2a \rho a^\dagger - a^\dagger a \rho - \rho a^\dagger a]. \end{aligned} \quad (2.7)$$

Here, $g_1 \equiv g c^2$ is the effective coupling constant between the dressed atom and the cavity. To determine the characteristics of the laser system, it is convenient to introduce density-matrix elements with respect to the two atomic dressed states, $\rho_{ij} \equiv \langle \tilde{i} | \rho | \tilde{j} \rangle$. These density-matrix elements obey the following equations of motion:

$$\dot{\rho}_{11} = g_1 (a^\dagger \rho_{21} + \rho_{12} a) - A_- \rho_{11} + A_+ \rho_{22} + \frac{1}{2} \kappa L_c \rho_{11}, \quad (2.8a)$$

$$\dot{\rho}_{22} = -g_1 (\rho_{21} a^\dagger + a \rho_{12}) + A_- \rho_{11} - A_+ \rho_{22} + \frac{1}{2} \kappa L_c \rho_{22}, \quad (2.8b)$$

$$\dot{\rho}_{12} = g_1 (a^\dagger \rho_{22} - \rho_{11} a^\dagger) - \left(2A_0 + \frac{A_-}{2} + \frac{A_+}{2} \right) \rho_{12} + \frac{1}{2} \kappa L_c \rho_{12}, \quad (2.8c)$$

$$\dot{\rho}_{21} = g_1 (\rho_{22} a - a \rho_{11}) - \left(2A_0 + \frac{A_-}{2} + \frac{A_+}{2} \right) \rho_{21} + \frac{1}{2} \kappa L_c \rho_{21}, \quad (2.8d)$$

where $L_c \rho_{ij} \equiv 2a \rho_{ij} a^\dagger - a^\dagger a \rho_{ij} - \rho_{ij} a^\dagger a$. Further, it is useful to use the following Hermitian operator combination [31]

$$\rho^{(1)} = \rho_{22} + \rho_{11}, \quad (2.9a)$$

$$\rho^{(2)} = \rho_{22} - \rho_{11}, \quad (2.9b)$$

$$\rho^{(3)} = \frac{1}{2} (a \rho_{12} + \rho_{21} a^\dagger), \quad (2.9c)$$

$$\rho^{(4)} = \frac{1}{2} (a^\dagger \rho_{21} + \rho_{12} a). \quad (2.9d)$$

We note that $\rho^{(1)} = \text{Tr}_a(\rho)$ is the reduced density operator of the cavity. From Eqs. (2.8) one obtains the equations of motion for $\rho^{(i)}$ in the form

$$\dot{\rho}^{(1)} = -2g_1 \rho^{(3)} + 2g_1 \rho^{(4)} + \frac{1}{2} \kappa L_c \rho^{(1)}, \quad (2.10a)$$

$$\dot{\rho}^{(2)} = -2g_1 \rho^{(3)} - 2g_1 \rho^{(4)} - 2\gamma_2 \rho^{(1)} - 2\gamma_{\text{pop}} \rho^{(2)} + \frac{1}{2} \kappa L_c \rho^{(2)}, \quad (2.10b)$$

$$\begin{aligned} \dot{\rho}^{(3)} = & \frac{g_1}{4} (\rho^{(1)} a a^\dagger + a^\dagger a \rho^{(1)} - 2a \rho^{(1)} a^\dagger) \\ & + \frac{g_1}{4} (\rho^{(2)} a a^\dagger + a a^\dagger \rho^{(2)} + 2a \rho^{(2)} a^\dagger) - \gamma_{\text{coh}} \rho^{(3)} - \frac{\kappa}{2} \rho^{(3)} \\ & + \frac{1}{2} \kappa L_c \rho^{(3)}, \end{aligned} \quad (2.10c)$$

$$\begin{aligned} \dot{\rho}^{(4)} = & -\frac{g_1}{4} (\rho^{(1)} a^\dagger a + a^\dagger a \rho^{(1)} - 2a^\dagger \rho^{(1)} a) \\ & + \frac{g_1}{4} (\rho^{(2)} a^\dagger a + a^\dagger a \rho^{(2)} + 2a^\dagger \rho^{(2)} a) - \gamma_{\text{coh}} \rho^{(4)} + \frac{\kappa}{2} \rho^{(4)} \\ & - \kappa \rho^{(3)} + \frac{1}{2} \kappa L_c \rho^{(3)}, \end{aligned} \quad (2.10d)$$

where

$$\gamma_{\text{pop}} \equiv \frac{1}{2} (A_+ + A_-), \quad (2.11)$$

$$\gamma_2 \equiv \frac{1}{2} (A_+ - A_-), \quad (2.12)$$

$$\gamma_{\text{coh}} \equiv \frac{1}{2}(4A_0 + A_+ + A_-). \quad (2.13)$$

Note that γ_{pop} and γ_{coh} are the resonance fluorescence decay rates for the atomic populations and coherences, respectively [24,29].

The advantage of using the operator combinations (2.9) is now evident. Due to the dependence of Eq. (2.10) only on bilinear combinations of the cavity field operators, it is possible to decouple the equations in the photon-number representation for the diagonal elements $P_n^{(i)} \equiv \rho_{nn}^{(i)}$ and the off-diagonal elements $\rho_{nm}^{(i)}$. From Eqs. (2.10) it is obtained

$$\dot{P}_n^{(1)} = -2g_1 P_n^{(3)} + 2g_1 P_n^{(4)} + \kappa(n+1)P_{n+1}^{(1)} - \kappa n P_n^{(1)}, \quad (2.14a)$$

$$\begin{aligned} \dot{P}_n^{(2)} = & -2g_1 P_n^{(3)} - 2g_1 P_n^{(4)} - 2\gamma_2 P_n^{(1)} \\ & - (2\gamma_{\text{pop}} + \kappa n)P_n^{(2)} + \kappa(n+1)P_{n+1}^{(2)}, \end{aligned} \quad (2.14b)$$

$$\begin{aligned} \dot{P}_n^{(3)} = & \frac{g_1}{2}(n+1)(P_n^{(1)} - P_{n+1}^{(1)} + P_n^{(2)} + P_{n+1}^{(2)}) \\ & - \gamma_{\text{coh}} P_n^{(3)} - \frac{\kappa}{2}P_n^{(3)} + \kappa(n+1)P_{n+1}^{(3)} - \kappa n P_n^{(3)}, \end{aligned} \quad (2.14c)$$

$$\begin{aligned} \dot{P}_n^{(4)} = & \frac{g_1}{2}n(P_{n-1}^{(1)} - P_n^{(1)} + P_{n-1}^{(2)} + P_n^{(2)}) - \gamma_{\text{coh}} P_n^{(4)} + \frac{\kappa}{2}P_n^{(4)} \\ & - \kappa P_n^{(3)} + \kappa(n+1)P_{n+1}^{(4)} - \kappa n P_n^{(4)}. \end{aligned} \quad (2.14d)$$

III. NONCLASSICAL EFFECTS

In what follows, we investigate the phenomena of photon antibunching and sub-Poissonian photon statistics, which are two distinct signatures of nonclassical states of light [32], i.e., states that have no description in terms of electromagnetic waves. For n photodetections of a stationary field, the photon counting statistics are super- or sub-Poissonian if $\langle(\Delta n)^2\rangle$ exceeds or not $\langle n \rangle$ [32]. For coherent states, $\langle(\Delta n)^2\rangle = \langle n \rangle$, and the photon statistics is Poissonian. The departure from the Poissonian statistics is measured by the Mandel q parameter [33] (normalized variance), defined by

$$q = \frac{\langle n^2 \rangle - \langle n \rangle^2}{\langle n \rangle} - 1. \quad (3.1)$$

This is related to the second-order coherence function $g^{(2)}(0) = (\langle n^2 \rangle - \langle n \rangle^2) / \langle n \rangle^2$ by $q = [g^{(2)}(0) - 1] \langle n \rangle$. For sub-

Poissonian photon statistics, $q < 0$ [or, equivalently, $g^{(2)}(0) < 1$], while for super-Poissonian statistics, $q > 0$ [or $g^{(2)}(0) > 1$].

The photon antibunching effect is described in terms of the normalized two-time second-order correlation function

$$g^{(2)}(t) = \frac{\langle a^\dagger a^\dagger(t) a(t) a \rangle_s}{\langle a^\dagger a \rangle_s^2}, \quad (3.2)$$

where s indicates steady-state averages, and the operators without time argument refer to their values at $t=0$. $g^{(2)}(t)$ measures the probability of detecting a second photon a time t after a first photon has been detected [34]. Photon antibunching represents the tendency of photons to distribute themselves individually rather than in bunches, so fewer photons pairs are detected close together than further apart. Photon bunching is the opposite effect, in which more photons distribute themselves in bunches, and more photon pairs are detected closer together than further apart. Therefore, photon antibunching implies that the probability of detecting two photons separated by a time t increases with increasing t from $t=0$, and is defined by

$$g^{(2)}(0) < g^{(2)}(t). \quad (3.3)$$

This condition violates the Schwartz inequality for a field obeying classical statistics, and is a characteristics of a quantum (nonclassical) field. Equivalently, the photon bunching is defined by $g^{(2)}(0) > g^{(2)}(t)$.

A. Photon statistics of the cavity field

The cavity field photon statistics can be investigated using the steady-state photon-number distribution $\bar{P}_n \equiv \bar{P}_n^{(1)}$ (where $\bar{P}_n^{(i)}$ is the steady-state value of $P_n^{(i)}$). This is obtained by solving the system of equations (2.14) in steady state, which corresponds to setting $\dot{P}_n^{(i)} = 0$, $i=1,4$. From Eq. (2.14a), we obtain

$$\bar{P}_n^{(3)} = \bar{P}_{n+1}^{(4)} = \frac{\kappa}{2g_1}(n+1)\bar{P}_{n+1}. \quad (3.4)$$

Using this result and Eqs. (2.14b) and (2.14d), we obtain

$$\begin{aligned} \bar{P}_n^{(2)} = & -\frac{\kappa^2}{g_1^2} \frac{\kappa(n+1)(n+2)}{2\gamma_{\text{pop}} + \kappa(2n+1)} \bar{P}_{n+2} \\ & + \frac{\kappa^2(n+1)}{g_1^2} \frac{2\gamma_{\text{coh}} + \kappa(2n+1)}{2\gamma_{\text{pop}} + \kappa(2n+1)} \bar{P}_{n+1} \\ & - \frac{2\gamma_2 + \kappa(2n+1)}{2\gamma_{\text{pop}} + \kappa(2n+1)} \bar{P}_n \end{aligned} \quad (3.5)$$

and

$$\begin{aligned} & \frac{\kappa^2}{g_1^2} \frac{\kappa(n+3)(n+2)}{2\gamma_{\text{pop}} + \kappa(2n+3)} \bar{P}_{n+3} - \frac{\kappa^2}{g_1^2} (n+2) \left(\frac{2\gamma_{\text{pop}} + \kappa n}{2\gamma_{\text{pop}} + \kappa(2n+1)} + \frac{1}{2} \frac{2\gamma_{\text{coh}} + \kappa(2n+3)}{2\gamma_{\text{pop}} + \kappa(2n+3)} \right) \bar{P}_{n+2} \\ & + \left(\frac{\kappa^2}{g_1^2} \frac{2\gamma_{\text{pop}} + \kappa n}{2\kappa} \frac{2\gamma_{\text{coh}} + \kappa(2n+1)}{2\gamma_{\text{pop}} + \kappa(2n+1)} + \frac{2(\gamma_{\text{pop}} + \gamma_2) + 2\kappa(2n+3)}{2\gamma_{\text{pop}} + \kappa(2n+3)} \right) \bar{P}_{n+1} - \frac{2(\gamma_{\text{pop}} - \gamma_2)}{2\gamma_{\text{pop}} + \kappa(2n+1)} \bar{P}_n = 0. \end{aligned} \quad (3.6)$$

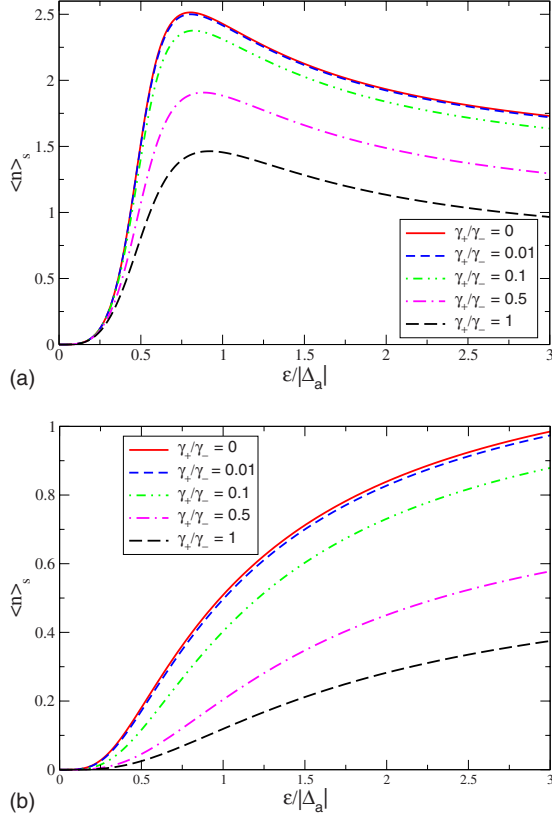


FIG. 2. (Color online) Mean cavity photon number as a function of the scaled driving field Rabi frequency, $\varepsilon/|\Delta_a|$, for various values of the jump in the photonic DOS, γ_+/γ_- , in the absence of dipolar dephasing ($\gamma_p=0$), and for negative (a) and positive (b) detuning Δ_a between the atomic resonant frequency and the driving field frequency. We have set $\kappa=0.1\gamma_-$ and $g=10\kappa$ in the calculations.

The photon-number distribution function \bar{P}_n is obtained by solving the system of Eq. (3.6). This is done by truncating the photon number such that \bar{P}_n does not change as the number of the truncated states is increased. The statistical properties of the cavity field is then investigated in terms of Mandel q parameter (3.1), where

$$\langle n \rangle = \sum_{n \geq 0} n \bar{P}_n, \quad (3.7)$$

$$\langle n^2 \rangle = \sum_{n \geq 0} n^2 \bar{P}_n. \quad (3.8)$$

Figures 2 and 3 present the intracavity photon number and normalized Mandel q parameter, respectively, as functions of the driving field intensity for various values of the discontinuity in the photonic density of states, ranging from the case of a cavity engineered in a photonic crystal with a full photonic band gap ($\gamma_+/\gamma_- = 0$) to the case of a cavity in ordinary vacuum ($\gamma_+/\gamma_- = 1$), in the absence of dipolar dephasing, and in the good cavity limit, $\kappa=0.1\gamma_-$. For $\gamma_- = 100\gamma$, this value of the cavity decay rate corresponds to a cavity quality factor of the order of 10^5 . Such cavity quality factors have been realized in 2D photonic-crystal slabs [22]. We obtain that for negative atom-driving field detuning the emission in cavities

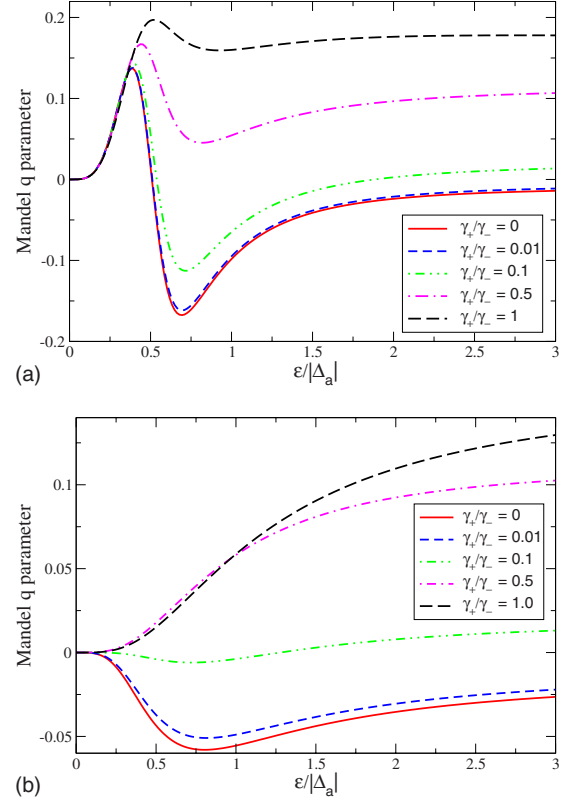


FIG. 3. (Color online) Mandel q parameter as a function of the scaled driving field Rabi frequency, $\varepsilon/|\Delta_a|$, for various values of the jump in the photonic DOS, γ_+/γ_- , in the absence of dipolar dephasing ($\gamma_p=0$), and for negative (a) and positive (b) detuning Δ_a between the atomic resonant frequency and the driving field frequency. We have set $\kappa=0.1\gamma_-$ and $g=10\kappa$ in the calculations.

engineered in photonic structures with large discontinuities in the photonic density of states is enhanced with respect to that for conventional cavities and is characterized by pronounced sub-Poissonian statistics. In contrast, in conventional cavities, the emission is super-Poissonian. Also, the cavity field mean photon number as a function of the driving field intensity exhibits a maximum that is accompanied by a minimum of the Mandel q parameter (strong quantum noise reduction). The nonclassical effect and the cavity field intensity decrease at large pump intensities, similarly with the experimental observations for a conventional one-atom laser realized with a four-level atomic system and a more elaborated pumping scheme [4]. The emission enhancement and sub-Poissonian photon statistics in photonic-crystal cavities are also present in the case of positive atom-driving field detuning, only in this case the number of photons in the cavity mode is smaller and the nonclassical effect is strongly reduced as compared to the case of positive detuning. Also, in this case, the cavity field intensity increases with the driving field. The dephasing processes have a deleterious effect on the photon emission, reducing the number of cavity photons and the nonclassical effect (which seems more sensitive to the effect of dephasing than the cavity field intensity), as presented in Fig. 4, but the general emission characteristics are preserved. We also note that quantitatively similar results are obtained for photonic structures characterized by a dis-

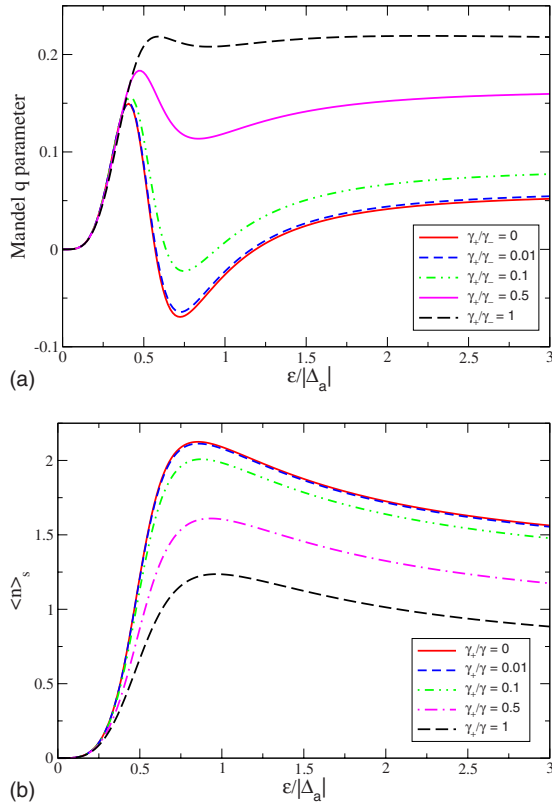


FIG. 4. (Color online) Mandel q parameter (a) and mean cavity photon number (b) as functions of the scaled driving field Rabi frequency, $\epsilon/|\Delta_a|$, for various values of the jump in the photonic DOS, γ_+/γ_- , in the presence of dipolar dephasing, $\gamma_p=0.05\gamma_-$, and for negative detuning Δ_a between the atomic resonant frequency and the driving field frequency. We have set $\kappa=0.1\gamma_-$ and $g=10\kappa$ in the calculations.

continuity in the photonic DOS of a factor of 100 ($\gamma_+/\gamma_-=0.01$) and photonic band-gap structures ($\gamma_+/\gamma_-=0$), which suggest that a photonic structure with a full photonic band gap may not be necessary to attain pronounced emission enhancement and sub-Poissonian photon statistics.

The emission characteristics presented above can be explained by noting that in the master equation (2.7) the term containing $A_-/2$ [equal to $(\gamma_-/2)s^4$ in the absence of dipolar dephasing] has the effect of pumping the atom from the lower dressed state $|\tilde{1}\rangle$ to the excited dressed state $|\tilde{2}\rangle$, while the term containing $A_+/2$ [equal to $(\gamma_+/2)c^4$ in the absence of dipolar dephasing] describes the relaxation of the atom from the excited dressed state $|\tilde{2}\rangle$ to the ground state $|\tilde{1}\rangle$. In the case of negative atom-driving field detuning, $c^4 < s^4$, the pumping process dominates that of relaxation, and a population inversion is created both in conventional cavities ($\gamma_+=\gamma_-$) and photonic-crystal cavities ($\gamma_+ \ll \gamma_-$). As a result, the process of stimulated emission into the cavity mode dominates the process of absorption of the cavity field, and this effect is more pronounced for photonic-crystal cavities, where the stronger “pumping” compared to the relaxation determines a larger dressed state atomic inversion. Therefore, the cavity photon number is enhanced for large discontinuities in the photonic density of states (or small γ_+/γ_-). Also,

similarly to a conventional laser, the cavity mean photon number is proportional to the product between the “pumping” rate $(\gamma_-/2)s^4$ and the coupling constant $g_1=gc^2$. For $\Delta_a < 0$, as a function of ϵ , this product presents a maximum and then decreases with increasing ϵ . As a result, the cavity photon number decreases after reaching a maximum at a driving field intensity that is independent of the photonic reservoir characteristics. On the other hand, for positive atom-driving field detuning, dressed atomic population inversion is produced only for driving field intensities above a certain value corresponding to the condition $\gamma_-s^4 > \gamma_+c^4$ and that increases with the decrease of the jump in the photonic density of states. Dressed atomic population inversion is absent in the case of conventional cavities. As a result, little or no net stimulated emission occurs for usual driving field intensities, and the cavity photon number is smaller than in the case of negative atom-driving field detuning. Also, in this case, the increase with the driving field intensity of the cavity field is caused by the increase of the product between the effective coupling constant g_1 and the “pumping rate” $(\gamma_-/2)s^4$ with the driving field intensity for all driving field intensities. The dephasing processes lead to an increase of the decay and “pumping” rates by the same amount (see the expressions of A_\pm), which explains the small change in the cavity intensity with the addition of dephasing.

Similarly, the emission statistical properties can be understood by analyzing the atomic excited state depopulation, described by the rate A_+ . This atomic decay is the analogous of spontaneous emission in a conventional laser. For conventional cavities or for photonic-crystal cavities engineered in structures characterized by small discontinuities in the photonic density of states, in the strong coupling limit $\kappa^2/g_1^2 \ll 1$, and the good cavity limit, $\kappa \ll \gamma_-$, all the terms of the order κ^2/g_1^2 and κ/γ_- in Eq. (3.6) can be neglected, and it is obtained

$$\bar{P}_n = \frac{s^4}{(\gamma_+/\gamma_-)c^4} \bar{P}_{n-1}. \quad (3.9)$$

This expresses the fact that the photon-number distribution function is a thermal distribution, characterized by super-Poissonian photon statistics. For a good cavity, the intensity fluctuations are averaged out, the photons leaving the cavity in a Poissonian process determined by κ . On the other hand, in the case of photon emission in cavities engineered in photonic structures characterized by large discontinuities in the photonic density of states ($\gamma_+ \ll \gamma_-$), it is possible to reduce (or even inhibit, in a photonic band-gap structure, where $\gamma_+=0$) the relaxation of the dressed atom from the dressed excited state to the ground state, such that, even for a good cavity, the dressed atomic decay rate is much smaller than the cavity decay rate, $(\gamma_+/2)c^4 \ll \kappa$. This leads to a photon-number distribution function characterized by sub-Poissonian photon statistics, similarly to the case of conventional one-atom lasers in bad cavities [23]. In this case, the emitted photons leave the cavity on a time scale shorter than the relaxation time and before undergoing any other processes. As a result, the photon emission preserves the properties of the regular atomic resonance fluorescence, charac-

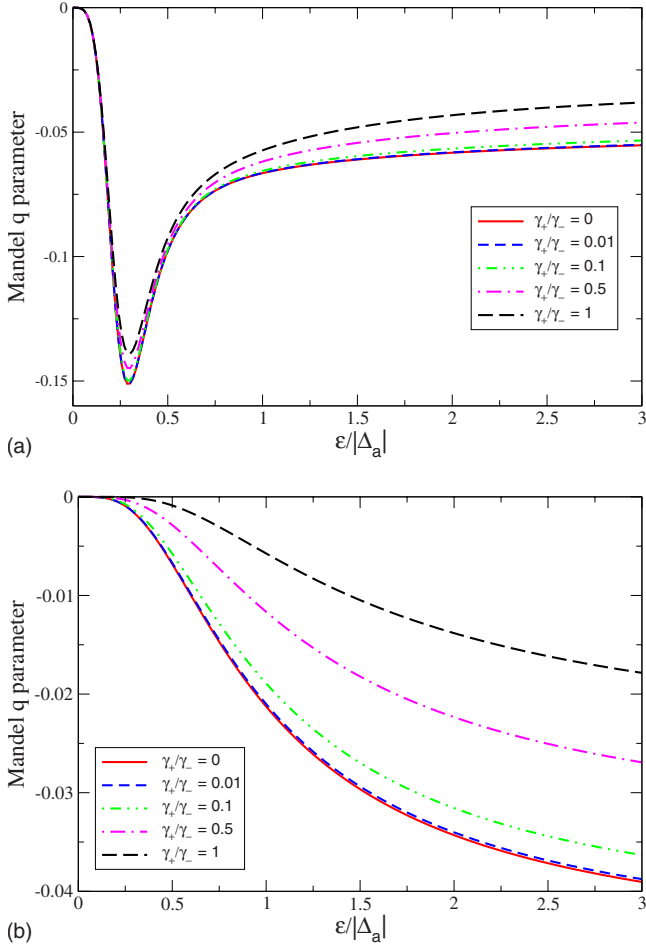


FIG. 5. (Color online) Mandel q parameter as a function of the scaled driving field Rabi frequency, $\epsilon/|\Delta_a|$, for various values of the jump in the photonic DOS, γ_+/γ_- , in the absence of dipolar dephasing, $\gamma_p=0$, for negative (a) and positive (b) detuning Δ_a between the atomic resonant frequency and the driving field frequency, and for a cavity decay rate $\kappa=\gamma_-$. The atom-cavity coupling constant has been set to $g=10\kappa$ in the calculations.

terized by sub-Poissonian photon statistics [35,29]. The dephasing processes increase the decay rate A_+ , and the system approaches the good cavity regime, resulting in a decrease in the nonclassical effect.

We note that (as also shown in Ref. [23]) sub-Poissonian photon statistics can be obtained for conventional cavities in the bad cavity limit, when the photon statistics are that of regular atomic resonance fluorescence. In this case, as presented in Fig. 5, the maximum amplitude squeezing in conventional cavities is comparable to that in good photonic-crystal cavities. However, the mean number of cavity photons in the bad cavity is much smaller than in a good cavity, as it can be seen from Figs. 2 and 6.

B. Photon antibunching

In order to investigate the antibunching effect, one needs to evaluate the two-time intensity correlation function

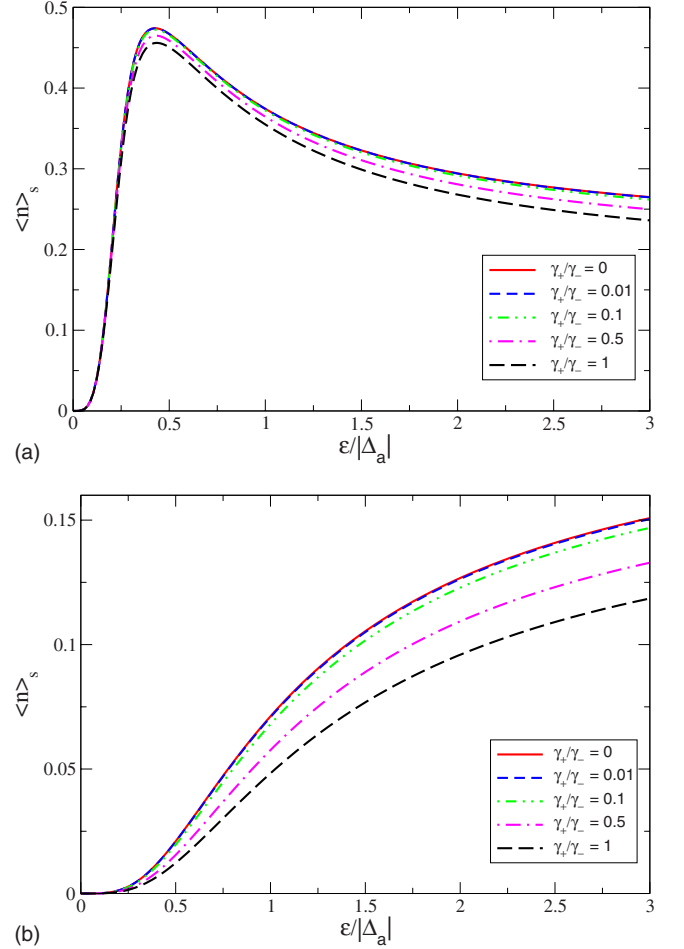


FIG. 6. (Color online) Mean cavity photon number as a function of the scaled driving field Rabi frequency, $\epsilon/|\Delta_a|$, for various values of the jump in the photonic DOS, γ_+/γ_- , in the absence of dipolar dephasing, $\gamma_p=0$, for negative (a) and positive (b) detuning Δ_a between the atomic resonant frequency and the driving field frequency, and for a cavity decay rate $\kappa=\gamma_-$. The atom-cavity coupling constant has been set to $g=10\kappa$ in the calculations.

$\langle a^\dagger a^\dagger(t)a(t)a \rangle_s$. Using that the time dependence of an operator O is given by $O(t)=U^\dagger(t)O(0)U(t)$, where $U(t)$ is the time evolution operator of the combined system of the cavity (c) plus atom (a) plus photonic reservoir (r), this two-time correlation function can be written as

$$\langle a^\dagger a^\dagger(t)a(t)a \rangle = \text{Tr}_{c,a,r}[a^\dagger U^\dagger(t)a^\dagger a U(t)a \rho_t], \quad (3.10)$$

where ρ_t is the density matrix of the total system of cavity (c) plus atom (a) plus reservoir (r). The expression (3.10) can be rewritten as

$$\langle a^\dagger a^\dagger(t)a(t)a \rangle_s = \text{Tr}_{c,a}[a^\dagger a \tilde{\rho}_{c,a}(t)], \quad (3.11)$$

where

$$\tilde{\rho}_{c,a}(t) = \text{Tr}_r[U(t)a \rho_t a^\dagger U^\dagger(t)] \quad (3.12)$$

is the reduced density matrix of the atom plus cavity. In the framework of the Markovian approximation, $\tilde{\rho}_{c,a}(t)$ obeys the same equation, Eq. (2.7), as the density operator $\rho(t)$ [36], but subject to the initial condition

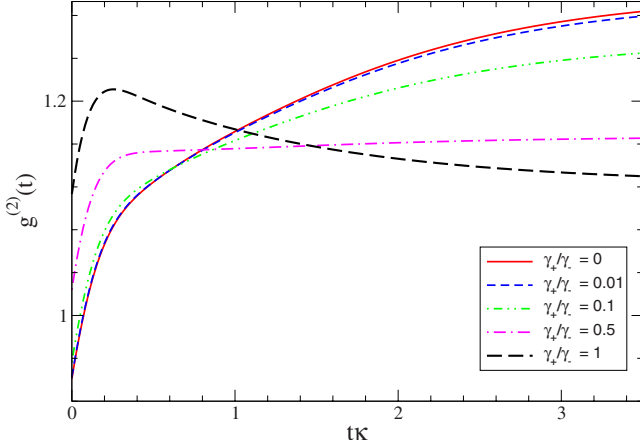


FIG. 7. (Color online) The quantum degree of second-order coherence $g^{(2)}(t)$ as a function of the scaled time $t\kappa$ for the scaled driving field Rabi frequency $\varepsilon/|\Delta_a|=0.75$, a cavity decay rate $\kappa=0.1\gamma_-$, negative detuning Δ_a between the atomic resonant frequency and the driving field frequency, and for various values of the discontinuity in the photonic density of states γ_-/γ_+ . The other parameters are the same as for Fig. 2.

$$\tilde{\rho}_{c,a}(0) = a(0)\rho(0)a^\dagger(0). \quad (3.13)$$

Analogously, in steady state,

$$\langle a^\dagger a^\dagger(t)a(t)a \rangle_s = \sum_{n \geq 0} n \tilde{P}_n^{(1)}(t), \quad (3.14)$$

where the quantities $\tilde{P}_n^{(i)}(t)$, $i=\bar{1},4$ satisfy the same equations, Eqs. (2.14) as $P_n^{(i)}(t)$, but are subject to the initial conditions

$$\tilde{P}_n^{(i)}(0) = (n+1)\bar{P}_{n+1}^{(i)}. \quad (3.15)$$

Thus, the two-time correlation function $\langle a^\dagger a^\dagger(t)a(t)a \rangle_s$ can be calculated according to (3.14) by solving the system of equations (2.14) subject to the initial conditions (3.15).

First, we note that for this one-atom laser system always $g^{(2)}(0) < g^{(2)}(t)$ near $t=0$, which expresses the fact that the emission is always characterized by photon antibunching. Indeed, using the definition (3.2) of the second-order coherence function, the expression (3.14), Eq. (2.14a), the initial condition (3.15), and the relationship (3.4), the time derivative of $g^{(2)}(t)$ at $t=0$ is expressed as

$$\dot{g}^{(2)}(0) = \kappa g^{(2)}(0) > 0. \quad (3.16)$$

The increase of $g^{(2)}(t)$ with t near $t=0$ is slower for photonic structures characterized by large discontinuities in the photonic density of states, when $g^{(2)}(0)$ is smaller, as it can be inferred from the results presented in the preceding section.

Figure 7 presents $g^{(2)}(t)$ as a function of the scaled delay time $t\kappa$, for a good cavity, $\kappa=0.1\gamma_-$, in the absence of dipolar dephasing, for various values of the discontinuity in the photonic density of states, γ_-/γ_+ , ranging from the case of a cavity engineered in a PBG material, $\gamma_-/\gamma_+=0$, to the case of

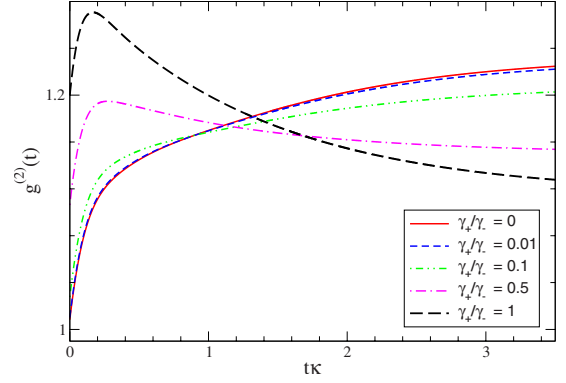


FIG. 8. (Color online) The quantum degree of second-order coherence $g^{(2)}(t)$ as a function of the scaled time $t\kappa$ in the presence of dipolar dephasing of $\gamma_p=0.1\kappa$. The other parameters are the same as for Fig. 7.

a cavity in free space, $\gamma_-/\gamma_+=1$. We consider negative detuning between the atomic resonant frequency and the driving field frequency, $\Delta_a < 0$, and the driving field intensity is set to $\varepsilon/|\Delta_a|=0.75$. This value corresponds to the maximum value of the cavity field intensity (as presented in Fig. 2). The cavity field exhibits photon antibunching both for conventional and photonic-crystal cavities, and the antibunching effect is still present even for relatively large dephasing, as shown in Fig. 8.

The photon antibunching effect in a one-atom laser system has the same origins as that in the single-atom resonance fluorescence [27], namely a time delay between the photon emission and atom reexcitation. After emitting a photon, the atom is in the ground state and it takes the driving field some time to reexcite the atom to the upper level to emit a next photon. Thus, the photons present a tendency toward antibunching for small delay times.

To understand the features in the time dependence of $g^{(2)}(t)$ presented in Fig. 7, we employ Eqs. (2.14a), (2.14b), (2.14c), and (2.14d) to derive an expression for the second-order time derivative of $g^{(2)}(t)$ at $t=0$. In the strong coupling limit $\kappa^2/g_1^2 \ll 1$, and the good cavity limit, $\kappa \ll \gamma_-$, all terms containing κ in Eqs. (2.14a), (2.14c), and (2.14d) can be neglected. Thus, we obtain

$$\ddot{\tilde{P}}_n^{(1)} = -2g_1(\dot{\tilde{P}}_n^{(3)} - \dot{\tilde{P}}_n^{(4)}), \quad (3.17)$$

where $\tilde{P}_n^{(3,4)}$ are given by Eqs. (2.14c) and (2.14d) where just the terms containing g_1 and γ_3 are present. Also, Eq. (3.5) can be reduced to $\bar{P}_n^{(2)} \approx -(\gamma_2/\gamma_{\text{pop}})\bar{P}_n^{(1)}$. Further, we evaluate $\ddot{\tilde{P}}_n^{(1)}$ at $t=0$ [that determines $\ddot{g}^{(2)}(t)$ at $t=0$, according to (3.14)] using the initial conditions (3.15). We obtain

$$\begin{aligned} \ddot{g}^{(2)}(0) = & -2 \left[g_1^2 \left(1 - \frac{2\gamma_-s^4}{\gamma_{\text{pop}}} - \frac{1}{\gamma_{\text{pop}}g^{(2)}(0)} \frac{1}{\bar{n}/(\gamma_-s^4)} \right) \right. \\ & \left. + \kappa\gamma_{\text{coh}} \right] g^{(2)}(0). \end{aligned} \quad (3.18)$$

Therefore, assuming that around $t=0$, $g^{(2)}(t) \approx at^2 + bt + c$, the

time scale over which the increase in $g^{(2)}(t)$ is observed can be estimated as

$$\begin{aligned} \tau &= -\frac{\dot{g}^{(2)}(0)}{\ddot{g}^{(2)}(0)} \\ &\approx \frac{1}{2\kappa} \frac{1}{(g_1/\kappa)^2 \left(1 - \frac{2\gamma_- s^4}{\gamma_{\text{pop}}} - \frac{1}{\gamma_{\text{pop}} g^{(2)}(0)} \frac{1}{\bar{n}/(\gamma_- s^4)} \right) + \gamma_{\text{coh}}/\kappa}. \end{aligned} \quad (3.19)$$

Over this time scale, the relative increase of $g^{(2)}(t)$ is

$$\begin{aligned} \frac{\Delta g^{(2)}(t)}{g^{(2)}(0)} &\approx \frac{1}{4(g_1/\kappa)^2 \left(1 - \frac{2\gamma_- s^4}{\gamma_{\text{pop}}} - \frac{1}{\gamma_{\text{pop}} g^{(2)}(0)} \frac{1}{\bar{n}/(\gamma_- s^4)} \right) + 4\gamma_{\text{coh}}/\kappa}. \end{aligned} \quad (3.20)$$

These quantities depend on the photonic reservoir through γ_{pop} , γ_{coh} , γ_- , and $g^{(2)}(0)$ [the ratio between the average number of cavity photons and the ‘‘pumping’’ rate, $\bar{n}/(\gamma_- s^4)$, depends weakly on the radiation reservoir]. The longer time scale over which the second-order coherence function increases with time and its larger relative increase around $t=0$ for photonic structures with large discontinuities in the photonic DOS result from the decrease of the population and coherence decay rates, γ_{pop} and γ_{coh} , and of $g^{(2)}(0)$, as well as from the increase of γ_- in these structures. This, in turn, is determined by the ability to alter the photonic DOS experienced by various atomic dressed state resonant transitions, as it was presented in Sec. II. The decrease of the population and coherence decay rates in photonic crystal also result in narrower Mollow resonance fluorescence spectral components relative to the resonance fluorescence in ordinary vacuum [29], and narrower one-atom photon-crystal laser spectrum [15]. The dephasing processes increase the decay rates γ_{pop} and γ_{coh} , decreasing both τ and $\Delta g^{(2)}(t)/g^{(2)}(0)$.

IV. CONCLUSIONS

We have investigated the possibility of nonclassical light generation by a photonic-crystal one-atom laser with coherent pumping. It is shown that the ability to engineer the quantum optical characteristics in coherent light-matter interactions through suitable photonic-crystal architectures facilitates enhanced nonclassical light generation. We have considered the case of the microcavity frequency tuned on resonance with one of the sidebands of Mollow atomic resonance fluorescence spectrum. For a microcavity embedded into a photonic crystal, in the strong coupling and good cavity regimes, the light generation is enhanced relative to that of a conventional cavity in ordinary vacuum, and is characterized by sub-Poissonian photon statistics. This is in contrast with the case of a microcavity in ordinary vacuum, where the photon statistics is sub-Poissonian only in the bad cavity regime. We have also investigated the phenomenon of

photon antibunching in the one-atom laser. It is shown that the cavity photons exhibit antibunching for both photonic-crystal and conventional cavities, and that the antibunching effect is more pronounced for cavities engineered in photonic structures characterized by large discontinuities in the photonic DOS. These results suggest that the photonic-crystal one-atom laser may be used as a source of intense nonclassical electromagnetic fields. We have argued that the distinct features of the photonic-crystal cavity field are a direct consequence of the possibility of suppressing atomic population and coherence decays, resulted, in turn, from the ability to engineer discontinuous changes with frequency of the photonic DOS.

The analysis presented here provides a rigorous picture of the one-atom laser characteristics in the regime of strong external laser fields. For a laser beam passing through a micron-scale waveguide channel, strong driving field intensities can be realized with nanoWatt pump power. By using strong laser fields, the Mollow spectral components of resonance fluorescence are driven away from the photonic DOS singularity, so that over the width of the individual spectral bands the photonic DOS is smooth, leading to a Markovian dynamics of the atomic system. For weaker fields, the DOS singularity may lead to non-Markovian effects in the atom-radiation reservoir interaction [37], which, in turn, may determine even more unusual spectral and statistical properties of the cavity field.

This study shows that in order for pronounced nonclassical effects in the light generation to be attained, a discontinuity of the photonic DOS of an order of 100 is enough, and a full-photon band gap is not necessary. This may bring some relaxation in the experimental realization of the system. Moreover, nonclassical effects of some degree can be observed even for a DOS jump of order 10. This can be achieved in 2D photonic-crystal microchips [38,14], for which tremendous experimental progress has been made recently, such that the system proposed here can reach the proof-of-principle stage in 2D photonic-crystal slabs using the already well-established fabrication and characterization techniques [22,17,8,16,18]. Furthermore, a great platform for electromagnetic vacuum engineering and photonic circuitry, the necessary ingredients for revealing the effects predicted here, is provided by 3D-2D-3D photonic heterostructures [20], in which a 2D photonic-crystal layer (comprising waveguides, microcavities) is clad by 3D photonic-crystal structure on both sides. These heterostructures also overcome the limitations of 2D photonic crystals, while retaining the design flexibility of a planar optical microchip. It was theoretically demonstrated that in 3D-2D-3D photonic heterostructures DOS jumps of order 100 or more over a very narrow frequency interval can be realized [21]. Various such photonic architectures have been proposed recently and theoretically demonstrated to enable true 3D photonic circuitry [20,39]. These theoretical advances have, in turn, motivated the experimental effort. Recently, the first 3D-2D-3D photonic heterostructure has been fabricated by direct laser writing [19], which represents the first step towards realizing the farther-reaching goal of fully implementing the effects predicted in this study.

ACKNOWLEDGMENTS

This work was performed at Jet Propulsion Laboratory, California Institute of Technology under contract with Na-

tional Aeronautics and Space Administration (NASA). The author acknowledges support from the National Research Council and NASA, Code S.

-
- [1] M. G. Raizen, R. J. Thompson, R. J. Brecha, H. J. Kimble, and H. J. Carmichael, *Phys. Rev. Lett.* **63**, 240 (1989).
- [2] G. Rempe, R. J. Thompson, R. J. Brecha, W. D. Lee, and H. J. Kimble, *Phys. Rev. Lett.* **67**, 1727 (1991).
- [3] Q. A. Turchette, C. J. Hood, W. Lange, H. Mabuchi, and H. J. Kimble, *Phys. Rev. Lett.* **75**, 4710 (1995).
- [4] J. McKeever, A. Boca, A. D. Boozer, J. R. Buck, and H. J. Kimble, *Nature (London)* **425**, 268 (2003).
- [5] J. McKeever *et al.*, *Science* **303**, 1992 (2004).
- [6] E. Yablonovitch, *Phys. Rev. Lett.* **58**, 2059 (1987).
- [7] S. John, *Phys. Rev. Lett.* **58**, 2486 (1987).
- [8] O. Painter *et al.*, *Science* **284**, 1819 (1999).
- [9] Sajeev John, *Phys. Rev. Lett.* **53**, 2169 (1984).
- [10] S. John and J. Wang, *Phys. Rev. Lett.* **64**, 2418 (1990).
- [11] S. John and Tran Quang, *Phys. Rev. A* **50**, 1764 (1994).
- [12] S. John and Tran Quang, *Phys. Rev. Lett.* **78**, 1888 (1997); S. John and M. Florescu, *J. Opt. A, Pure Appl. Opt.* **3**, S103 (2001).
- [13] Tran Quang, M. Woldeyohannes, S. John, and G. S. Agarwal, *Phys. Rev. Lett.* **79**, 5238 (1997); S. Y. Zhu, H. Chen, and Hu Huang, *ibid.* **79**, 205 (1997); D. G. Angelakis, E. Paspalakis, and P. L. Knight, *Phys. Rev. A* **64**, 013801 (2001); Y. V. Ros-tovtsev, A. B. Matsko, and M. O. Scully, *ibid.* **57**, 4919 (1998).
- [14] Lucia Florescu, Sajeev John, Tran Quang, and Rongzhou Wang, *Phys. Rev. A* **69**, 013816 (2004).
- [15] Lucia Florescu, *Phys. Rev. A* **74**, 063828 (2006).
- [16] D. Englund, D. Fattal, E. Waks, G. Solomon, B. Zhang, T. Nakaoka, Y. Arakawa, Y. Yamamoto, and J. Vuckovic, *Phys. Rev. Lett.* **95**, 013904 (2005).
- [17] Antonio Badolato *et al.*, *Science* **308**, 1158 (2005).
- [18] S. Strauf, K. Hennessy, M. T. Rakher, Y. S. Choi, A. Badolato, L. C. Andreani, E. L. Hu, P. M. Petroff, and D. Bouwmeester, *Phys. Rev. Lett.* **96**, 127404 (2006).
- [19] M. Deubel, M. Wegener, S. Linden, G. Von Freymann, and Sajeev John, *Opt. Lett.* **31**, 805 (2006).
- [20] A. Chutinan, Sajeev John, and O. Toader, *Phys. Rev. Lett.* **90**, 123901 (2003); Alongkarn Chutinan and Sajeev John, *Phys. Rev. E* **71**, 026605 (2005).
- [21] R. Z. Wang and Sajeev John, *Phys. Rev. A* **70**, 043805 (2004).
- [22] Y. Akahane, T. Asano, B. Song, and S. Noda, *Nature (London)* **425**, 944 (2003); Y. Akanane, T. Asano, B. S. Song, and S. Noda, *Opt. Express* **13**, 1202 (2005); B. S. Song, S. Noda, T. Asano, and Y. Akahane, *Nat. Mater.* **4**, 207 (2005).
- [23] Tran Quang and H. Freedhoff, *Phys. Rev. A*, **47**, 2285 (1993); H. Freedhoff and Tran Quang, *Phys. Rev. Lett.* **72**, 474 (1994).
- [24] C. Cohen-Tannoudji, J. Dupont-Roc, and S. Grynberg, *Atom-Photon Interactions* (Wiley-Interscience, New York, 1992).
- [25] B. R. Mollow, *Phys. Rev. A* **5**, 2217 (1972).
- [26] G. S. Agarwal, L. M. Narducci, Da Hsuan Feng, and R. Gilmore, *Phys. Rev. Lett.* **42**, 1260 (1979).
- [27] H. J. Carmichael, *Statistical Methods in Quantum Optics I* (Springer-Verlag, Berlin, 1999).
- [28] M. Florescu and S. John, *Phys. Rev. A* **64**, 033801 (2001).
- [29] Marian Florescu and Sajeev John, *Phys. Rev. A* **69**, 053810 (2004).
- [30] For frequency detunings of the order $\Delta_\omega \approx 10^8 \text{ s}^{-1}$, the electric field amplitudes E used in our calculations are of the order of a few kV/m. On the other hand, the intensity of an electromagnetic wave is the time average over the detector response time of the Poynting vector, describing the rate of flow of electromagnetic energy. For a plane wave, the intensity, I , and amplitude, E , of the electric field are related to each other by $I[\text{W/m}^2] \approx 1.33 \times 10^{-3} |E[\text{V/m}]|^2$. Thus, an electric field amplitude $E \approx 10^3 \text{ V/m}$, gives an intensity $I \approx 10^3 \text{ W/m}^2$. For a waveguide channel with cross-sectional area on the scale of $(\text{micron})^2$, this corresponds to a net power of about 1 nW.
- [31] T. Quang, P. L. Knight, and V. Buzek, *Phys. Rev. A* **44**, 6092 (1991).
- [32] X. T. Zou and L. Mandel, *Phys. Rev. A* **41**, 475 (1990).
- [33] L. Mandel, *Opt. Lett.* **4**, 205 (1979).
- [34] R. J. Glauber, *Phys. Rev.* **130**, 2529 (1963); **131**, 2766 (1963).
- [35] N. N. Bogolubov, Jr., E. I. Aliskenderov, A. S. Shumovsky, and T. Quang, *J. Phys. B* **20**, 1885 (1987).
- [36] C. W. Gardiner, *Handbook of Stochastic Methods* (Springer, Heidelberg, 1983).
- [37] N. Vats and S. John, *Phys. Rev. A* **58**, 4168 (1998).
- [38] A. A. Asatryan, K. Busch, R. C. McPhedran, L. C. Botten, C. M. de Sterke, and N. A. Nicorovici, *Phys. Rev. E* **63**, 046612 (2001).
- [39] Alongkarn Chutinan and Sajeev John, *Phys. Rev. B* **72**, 161316(R) (2005); *Opt. Express* **14**, 1266 (2006).